Novel Thiadiazoline Spiro Quinoline Analogues Induced Cell death in MCF-7 cells via G2/M Phase Cell Cycle Arrest

Selvaraj Shyamsivappan
Bharathiar University
Raju Vivek
Bharathiar University
Thangaraj Suresh
Bharathiar University
Adhigaman Kaviyarasu
Bharathiar University
Sundarasamy Amsaveni
Bharathiar University
Shunmuganarayanan Athimoolam
Anna University
Palathurai Subramaniam Mohan (psmohan59@gmail.com)
Bharathiar University

Research Article

Keywords: novel thiadiazoline spiro quinoline derivatives, thiadiazoline spiro quinoline derivatives, target validation

Posted Date: March 16th, 2021

DOI: https://doi.org/10.21203/rs.3.rs-289802/v1

Abstract

A progression of novel thiadiazoline spiro quinoline derivatives were synthesized from potent thiadiazoline spiro quinoline derivatives . The synthesized compounds portrayed by different spectroscopic studies and single X-ray crystallographic studies. The compounds were assessed for in vitro anticancer properties towards MCF-7 and HeLa cells. The compounds showed superior inhibition action MCF-7 malignant growth cells. Amongst, the compound 4a showed significant inhibition activity, the cell death mechanism was evaluated by fluorescent staining, and flow cytometry, RT-PCR, and western blot analyses. The in vitro anticancer results revealed that the compound 4a induced apoptosis by inhibition of estrogen receptor alpha (ERα) and G2/M phase cell cycle arrest. The binding affinity of the compounds with ERα and pharmacokinetic properties were confirmed by molecular docking studies.

Introduction

Cancer is one of the rapidly growing diseases and causes millions of deaths worldwide. Cervical and breast cancers are the most prevalent reason of cancer death in women.[1] Presently, radiotherapy and chemotherapy are the most effective cancer treatments. However, due to the toxicity and side effects of the currently available drugs, there is an emerging need for new targeting drugs with a various mechanism of actions. In the clinical samples, the most breast carcinoma cells express the estrogen receptor alpha (ERα).[2] ERα is a nuclear hormone which promotes the proliferation of the breast carcinoma cells. In the therapeutic view, ERα targeting therapy is one of the essential treatments in breast cancer patients.

In this therapeutic context, the sulfur and nitrogen-containing thiadiazole pharmacophores were widely used in the medicinal chemistry field for drug designing.[3,4] The recent reports have demonstrated that the thiadiazole incorporated heterocyclic scaffolds have significant inhibition effects against the proliferation of various cancer cell lines with different mechanisms of action. For example inverse agonist for estrogen receptor alpha ERα,[5] PPARγ peroxisome proliferators activated receptor co activator 1α signaling by ERα ligand,[6] inhibition of glutaminase 1,[7] inhibition of sphingosine kinase,[8] inhibition of c-Met,[9] inhibition of mitotic kinesin Eg5,[10] inhibition of Src hormology-2 domain-containing protein tyrosine phosphate-2,[11] suppression of IL-6/COX-2 intermediated JAK2/STAT3 signals,[12] etc.

The quinoline heterocycles are significant class compounds that are found in several natural products and synthetic scaffolds. The early reports discovered that the quinoline analogues inhibits the growth of cancer cells by targeted mechanism of action such as Estrogen receptor binding,[13] Estrogen receptor degrader,[14] topoisomerase 1 (Top1) inhibitors,[15] inhibition of histone deacetylase 6,[16] inhibition of c-KIT kinase,[17] ataxia telangiectasia mutated (ATM) kinase inhibition,[18] topoisomerase IIα (TOP2A) inhibition,[19] HSP90 inhibitors,[20] tubulin polymerization inhibitors, dihydroorotate dehydrogenase (hDHODH) inhibitors,[21] inhibition of AXL kinase,[22] Inhibition of mutant isocitrate dehydrogenase 1 (mIDH1),[23] inhibition of Rho-associated protein kinase (ROCK),[24] inhibition of aldehyde dehydrogense

1A1 (ALDH1A1),[25] etc. Because of these crucial activities of quinoline scaffolds, recently we have reported 8-nitroquinolone based compounds, that resulting good antitumor properties.[26-29]

Prompted by the early reports of the thiadiazole and quinoline motifs, herein, we synthesized a novel thiadiazoline spiro quinoline from 8-nitro quinoline thiosemicarbazones. All the synthesized thiadiazoline spiro quinoline compounds were assessed *in vitro* anticancer properties against HeLa and MCF-7 cells. Amongst, compound **4a** showed significant activity towards MCF-7 cells. The molecular cell death mechanisms were evaluated and the results confirmed that the compound **4a** prompted apoptosis by inhibition of estrogen receptor alpha (ERα) and G2/M phase cell cycle arrest in MCF-7 cells. Furthermore, pharmacokinetics properties and binding interaction between the compound and ERα protein were confirmed by docking studies.

Results And Discussion

Chemistry

New novel thiadiazoline spiro quinoline analogues were synthesized by two step reactions (**Scheme 1**). The initial reaction involves the synthesis of quinoline-thiosemicarbazones from the corresponding reaction between thiosemicarbazides **1a-d** and C-6 functionalized 8-nitro-2,3-dihydroquinolines **2a-c**. In the next step, the cyclization was carried out by the treatment of quinoline-thiosemicarbazones with acetic anhydride at 90 °C for 4 hours. The heterocyclization promotes the N-acetylation of the quinoline-thiosemicarbazones and afforded 1,3,4-thiadiazoline core of the spiro compounds in good yield.

Crystal Packing and Molecular Geometry of 4d

The two molecules of compound **4d** were crystallized in centrosymmetric triclinic unit cell. The combination of the structure was confirmed by R-factor of 6.34%. As indicated by Cremer and Pope analysis the thiadiazole ring adopted envelope conformation with the puckering coordinates of q_2 = 0.199(2) Å and f_2 = 30.76(1)° and the six-membered nitro-substituted heterocyclic ring adopts twisted boat conformation with the puckering coordinates of q_2 = 0.433(2) Å, f_2 = 219.96(1)° and q_3 = 0.279(2) Å. The phenyl and nitrophenyl rings are oriented with an angle of 13.2(2)° to each other. Further, the nitro group was bent out from phenyl ring plane with dihedral angle of 9.9(2)°. Two acetyl groups (-$COCH_3$) are twisted out from each with a dihedral angle of 21.9(5)° to one another. The hydrogen bonds geometry of the compound was showed in **table 1**.

Table 1. Geometry of hydrogen bonds (Å,°)

D-H···A	D(D-H)	d(H···A)	D(D···A)	<(DHA)
C16-H6···O3$^{\#1}$	0.96	2.63	3.549(8)	161
C16-H7···O2$^{\#2}$	0.96	2.56	3.166(8)	121
C18-H9···O3$^{\#3}$	0.93	2.64	3.336(9)	133
C20-H13···O2$^{\#4}$	0.96	2.53	3.379(8)	148
C21-H16···O3	0.97	2.42	2.956(6)	115
N2-H2N···O2	0.77(4)	2.03(4)	2.625(7)	133(3)
N2-H2N···O4$^{\#5}$	0.77(4)	2.58(4)	3.161(8)	134(3)

Symmetry transformation used to produce equivalent atoms:

#1 x, y+1, z; #2 x, y+1, z-1; #3 -x+2, -y+1, -z+1; #4x, y, z-1; #5 -x+2, -y+1, -z+2;

The crystal packing was conquered by non-classical C-H···O and classical N-H···O interactions. The intra- and intermolecular interaction can be destroyed by the graph-set motif for better understanding of any supramolecular architecture (**Figure 2**). In this context, the intermolecular interactions which connect the molecules in crystalline lattices are explained with graph set notation.[30]

The classical intramolecular hydrogen bond prompts to self-related S(6) motif through N2-H2N…O2 interactions. Further, two centro-symmetrically related intermolecular interactions are formed through C-H…O interactions leading to ring $R_2^2(20)$ and $R_2^2(24)$ motifs in the reversal centers of unit cell (**Figure 3a & 3b**). Further, these cento-symmetrically connected dimeric rings linked along *b*-axis and *bc*-diagonal of the unit cell leading to chain C(9) and C(10) motifs (**Figure 3c & d**). Further, the crystal packing features C-H…p and p…p interactions.

Plausible Reaction Mechanism for Formation of Desired Compounds

A plausible mechanism of compound **4a-l** with acetic anhydride is shown in **Scheme 2**. Initially, nucleophilic substitution with acetic anhydride on the NH group of **3a-l** followed by the cyclization forms the mono acetyl intermediates II. And then the intermediates II gradually converted into diacetyl thiadiazoline compounds **4a-l.**

In Vitro Anticancer Properties of Thiadiazoline Spiro Quinoline Analogues

The recent reports revealed that the thiadiazole and quinolines are promising compounds which showed good anticancer activity towards tumor cells. Recently we have reported a new thiosemicarbazones, spiro pyrrolo oxindoles, indenoquinoxalines and pyarn derivatives from 8-nitroquinolones that exhibited potential activity towards the cervical and breast cancer cells.[26-29] Hence, we selected specified cancer cell lines HeLa and MCF-7 to evaluate the cytotoxicity properties of the thiadiazoline spiro quinoline derivatives **4a-l**. The toxicity of the compounds was evaluated by using MCF10A non-tumorigenic epithelial breast cells.

Initially, to evaluate the toxicity, various concentrations of the thiadiazoline spiro quinolines were treated with MCF10A normal breast cells. The compounds did not showed any significant toxicity up to 100 µM concentrations towards normal cells. Hence, to examine the cytotoxicity of the compounds, we used less than 100 µM of concentrations of compounds towards the cancer cells. The anticancer medication doxorubicin was utilized as positive control to analyze anticancer impacts of the compounds. The MTT assay was performed to examine the inhibitory impacts **4a-l** towards proliferation of HeLa and MCF-7 cells. The outcomes were summarized by IC_{50} values that show the required concentration to inhibit the growth of 50% cells (**Table 2**).

Table 2. Anticancer MTT assay of 4a-l towards HeLa and MCF-7 cells

S.No.	Compounds	R	R_1	IC_{50} of HeLa (µM)	IC_{50} of MCF-7 (µM)
1	**4a**	**H**	**H**	**18.16±0.87**	**10.21±1.35**
2	4b	CH_3	H	22.24±1.43	17.53±1.29
3	4c	CH_2CH_3	H	24.63±0.86	21.22±1.42
4	4d	C_6H_5	H	26.35±0.78	23.38±0.78
5	4e	H	CH_3	22.11±1.35	17.81±0.41
6	4f	CH_3	CH_3	18.26±1.18	16.12±1.32
7	4g	CH_2CH_3	CH_3	19.31±1.32	18.26±1.23
8	4h	C_6H_5	CH_3	24.24±0.91	24.42±1.34
9	4i	H	Cl	26.36±1.24	18.72±0.79
10	4j	CH_3	Cl	29.14±0.79	22.16±0.82
11	4k	CH_2CH_3	Cl	31.62±0.36	28.64±1.13
12	4l	C_6H_5	Cl	38.71±1.13	34.21±0.57
Control	Dox	-	-	17.26±1.21	15.15±1.12

The MTT cytotoxicity results of the compounds showed potential inhibition activity towards the growth of the MCF-7 cells (IC_{50}<34.21±0.57 µM) and ERα negative HeLa cells (IC_{50}< 38.71±1.13 µM). Amongst, the compound **4a** showed maximum inhibitory activity against MCF-7 cells (10.21±1.35) and HeLa cells (18.16±0.87). Further, the compounds are more active against MCF-7 cells when compared with HeLa cells.

Structure-Activity Relationship (SAR)

The structure-activity relationship was explored to understand the cytotoxic impacts of substitutions on the tested compounds. From the MTT results the parent unsubstituted compound **4a** showed better inhibition activity towards the proliferation of the cancer cells (MCF-7 IC_{50} 10.21±1.35 and HeLa IC_{50} 18.16±0.87). On the examination of the effects of R substitution, the hydrogen substituted derivatives **4a**, **4e**, **4i** (MCF-7 IC_{50} 10.21±1.35 < 18.72±0.79 and HeLa IC_{50} 18.16±0.87 < 26.36±1.24) were

showed more potential inhibition activity than other ethyl and methyl and phenyl substitutions. On the observation of R_1 of the compounds, it was clear that the methyl and hydrogen substituted compounds showed better activity than chlorine substituted compounds. From the above perceptions, the order of inhibition activity of R substitution is H>CH_3>CH_3CH_2 >C_6H_6 and R1 substitution is H□CH_3□ Cl. The compounds are more active against MCF-7 cells when compared with HeLa cells. Hence, we selected the potent compound **4a** to examine mechanistic action towards MCF-7 cells.

Cell Morphology Analysis

The potent compound **4a** was treated with breast cancer MCF-7 cells in two different concentrations (25μM & 50μM). The phase-contrast microscopy was used record the cell morphology changes. The compound **4a** treated cells showed morphological changes like rounded, contracted and divided cell morphology whereas, the control cells exhibited usual morphology (**Figure 4**). The morphology change of the cells showed that the compound 4a was prompted cell death in tested MCF-7 cells.

Apoptotic Cell Death Detection by Acridine Orange/ Ethidium Bromide (AO/EB)

The apoptosis provoked in the tested cancer cell was examined by acridine orange/ ethidium bromide (AO/EB) dual staining method. The MCF-7 cells were treated with 25μM and 50μM of the compound **4a** for 24 hours and stained with AO/EB for 1 hour. The apoptotic morphology of the cells was examined in fluorescence microscopy. The fluorescence images showed orange stained cells with apoptotic fragmented, condensed chromatin nuclear morphology that showed late and early apoptotic dead cells. However, the non-treated control MCF-7 cells showed green fluorescence with usual morphology (**Figure 5**). The results revealed that the **4a** prompted apoptotic cell death in treated MCF-7 cells.

DAPI Staining Analysis for Discovery of Nuclear Damaged Apoptotic Cells by DAPI

DAPI is the dye that ties strongly with damaged nuclear DNA and emits blue fluorescence.[31] The MCF-7 cells were treated with 25μM and 50μM of the compound **4a** for 24 hours and stained with DAPI for 1 hour. The nuclear damage morphology in the treated cells was examined by fluorescence microscopy. In the fluorescence microscopy images the compound treated cells were appeared with condensed chromatin and fragmented nuclear morphology and emit bright blue fluorescence (**Figure 6**). However, the non-treated control MCF-7 cells showed normal morphology with less blue fluorescence. The results exposed that the compound **4a** damaged nuclear DNA and prompted cell death in MCF-7 cells.

Cell Cycle Analysis

Flow cytometry cell cycle method was used to determine the cell cycle in tested MCF-7 cells. The MCF-7 cells were treated with the compound **4a** in IC_{50} concentration and then the cell cycle was investigated. The control untreated cells were exhibited 62.11% of cells in G0-G1 phase, 18.70% of cell in

G1/S phase, and 15.18% of cells in G2/M phase. But the treated cells exhibited 21.44% of cell in G0-G1 phase, 9.47% of cells in G1/S phase, and 67.67% of cell in G2/M phase (**Figure 7**). From the flow cytometry results it was observed that the G2/M phase cells were extensively increased in tested cells. However, the G0-G1 and G1/S phase cells were reduced in treated cells. The cell cycle results exposed that the compound **4a** prompted cell cycle arrest in G2/M phase.

Annexin V- FITC and PI Staining Assay

The flow cytometry annexin V- FITC and PI staining method were employed to quantify died cells. The IC_{50} concentration of the compound **4a** was ERα positive MCF-7 cells and stained with annexin V-FITC and PI. Afterward the stained cells and untreated control cells were analyzed by flowcytometer. The results showed 62.99 percentage of necrotic cells, 0.30 percentage of late apoptotic cells and 0.33 percentage of early apoptotic cells (**Figure 8**). From the results, it was confirmed that the compound **4a** induced cell death MCF-7 cells.

Inhibition of Estrogen Receptor ERα by compound 4a

Estrogen Receptor ERα is one of the hormone that promotes the proliferation of breast carcinoma cells.[32] ERα targeting therapy is one of the essential therapies for breast cancer treatment. Commonly, the compound binds with the ERα results in the decrease of mRNA levels of ERα. Hence, we have investigated levels of ERα mRNA in the 4a treated cells. The well-known ERα positive breast cancer drug tamoxifen was utilized as positive control to evaluate the inhibiting ability of **4a**. The ERα positive MCF-7 cells were treated with the compound **4a** in IC_{50} concentration. Afterward the the ERα levels were determined by RT-PCR. The results showed significant decrease of ERα mRNA in treated cells (**Figure 9**).

The inhibition of ERα by **4a** was further confirmed by western blot analysis. After treatment, the proteins were taken out from the cells and the ERα levels were examined. The western blot results revealed that the compound **4a** was significantly inhibiting the ERα levels in the treated cells which are similar to the standard Tamoxifen results (**Figure 9c**). The results revealed that that the compound **4a** induced cell death by inhibition of ERα. From the above *in vitro* cytotoxic results, we conclude that the compound **4a** induced apoptosis by G2/M phase cell cycle arrest and inhibition of estrogen receptor alpha (ERα) in MCF-7 cells.

Molecular Interaction of ERα with Compounds

Further, the interactions of the compounds with breast cancer ERα protein was examined by computational docking studies. The ERα protein was downloaded from Protein data bank PDB with the ID of 3ERT. The Schrodinger maestro module protein making wizard was used to set up the PDB structure,[33] and Schordinger ligPrep module was employed to prepare the compound structures.[34] The prepared compounds and the protein structures were exposed to molecular docking by using Glide module.[35]

The results of the thiadiazoline spiro quinolines **4a-l** showed better binding affinities with estrogen receptor alpha protein (**Table 3**). Amongest the compound **4a** showed the most elevated binding affinity with a glide score of -5.925. The compound **4a** showed hydrogen bonding interaction with ERα residues of CYS530, LEU 546 through acetyl group and a nitro group of the compound (**Figure 10**). The compounds 4i, 4d, and 4f, also showed good binding affinities by forming hydrogen bonding interaction with ERα.

Table 3. The interaction between ERα receptor 3ERT with the compounds **4a-l** by molecular docking studies

Compounds	Glide gscore	Glide evdw	Glide ecoul	Glide energy	Interacting Residues
4a	-5.925	-33.787	-8.803	-42.589	CYS530, LEU 546, H_2O
4b	-4.245	-31.419	-4.754	-36.173	CYS530
4c	-4.803	-32.024	-5.237	-37.261	CYS530, H_2O
4d	-4.448	-36.621	-4.904	-41.524	CYS530, LEU 546
4e	-3.517	-30.621	-0.734	-31.355	-
4f	-4.833	-32.946	-6.449	-39.395	CYS530, LEU 546, H_2O
4g	-3.587	-32.257	-0.974	-33.231	-
4h	-4.531	-34.879	-4.703	-39.582	LEU 546
4i	-4.873	-37.331	-3.059	-40.390	H_2O
4j	-4.570	-32.540	-5.840	-38.379	CYS530, LEU 546, H_2O
4k	-4.769	-34.993	-3.764	-38.756	CYS530
4l	-3.960	-33.776	-4.973	-38.749	CYS530, LEU 546

Pharmacokinetic Studies

The drug-like ADME (adsorption, distribution, metabolism, and excretion) properties, Lipinski and Jorgensen rules were examined by pharmacokinetic studies using computational Qikprop module of Schrodinger.[36] The Lipinski's rules states that the molecular weight of the drug should be less than 500, the hydrogen bond donor of the drug should be ≤5, hydrogen bond acceptor of the drug should be ≤10, and the octanol / water partition coefficient ($QPlogP_{o/w}$) should be less than <5. The computational results of the compounds were satisfied the above rules (**Table 4**). Particularly, the potent compound **4a** showed the molecular weight is 349.364 a.m.u., hydrogen bond donor is 2, hydrogen bond acceptor is 8 and the octanol/water partition coefficient is 0.8. These results revealed that the compound **4a** fulfilled the Lipinski's rules.

The Jorgensen's drug-like rules are the solubility in water QPlogS should be greater than -5.7, the cell permeability of Caco-2 QPP Caco value should be greater than 22nm/s, and the primary metabolic reaction value #metab 7 values should be less than 7. The computational results of the compounds were satisfied the above rules (**Table 4**). The selected active compound **4a** fulfilled the rules with the QPlogS value of -3,669, QPP Caco value of 66.525, and #metab value of 4. The above results indicated that the compound **4a** is orally available.

Table 4. Pharmacokinetic Lipinski's and Jogensen's properties of the compound **4a-l**

Compounds	mol W <500	Donor HB <5	Acceptor HB <10	Qp log $P_{o/w}$ <5	QP log S > -5.7	QPP Caco > 22 nm/s	#metab < 7
4a	349.364	2	8	0.8	-3.669	66.525	4
4b	363.39	1	8.5	1.051	-3.56	105.852	4
4c	377.417	1	8.5	1.397	-3.819	119.131	4
4d	425.461	1	8.5	2.343	-4.807	127.661	5
4e	363.39	2	8	1.078	-4.152	66.155	4
4f	377.417	1	8.5	1.335	-3.98	105.128	4
4g	391.444	1	8.5	1.691	-4.29	119.611	4
4h	439.488	1	8.5	2.631	-5.171	128.531	5
4i	383.809	2	8	1.43	-4.402	99.603	3
4j	397.835	1	8.5	1.724	-4.304	182.623	3
4k	411.862	1	8.5	2.167	-4.75	207.96	3
4l	459.906	1	8.5	3.028	-5.551	205.582	4

Further, the synthesized compounds fulfilled the additional properties like QP log HERG values, partition coefficient of brain/blood QP log BB, the permeability of MDCK cell QPP MDCK, permeability of skin Qp log Kp, blood serum albumin binding capacity QP log Ksha, percentage of oral absorption, and Vander wall's polar surface area of oxygen and nitrogen atoms PSA (**Table 5**). The results demonstrated that the compounds having drug like properties with strong with strong binding sites.

Table 5. The pharmacokinetic properties of the thiadiazoline spiro quinolines **4a-l**

Compounds	QP log HERG < -5	QP log BB -3.0 to 1.2	QPP MDCK <25 poor, >500 great	QP logKp -8.0 to -1.0	QP logKhsa -1.5 to 1.5	Percent Human oral Absorption <25% is low >80% is high	PSA 7.0 to 200.0
4a	-4.307	-1.567	37.539	-5.207	-0.222	64.257	137.347
4b	-4.206	-1.385	55.534	-4.86	-0.258	69.337	128.638
4c	-4.374	-1.448	60.228	-4.657	-0.173	72.279	128.135
4d	-5.456	-1.501	65.909	-4.028	0.122	78.356	127.364
4e	-4.259	-1.633	37.313	-5.399	-0.095	65.839	137.364
4f	-4.071	-1.417	55.07	-5.042	-0.119	70.948	128.673
4g	-4.278	-1.487	60.602	-4.834	-0.031	74.037	127.996
4h	-5.207	-1.504	66.311	-4.219	0.27	80.1	127.44
4i	-4.318	-1.272	150.856	-5.01	-0.127	71.081	132.67
4j	-4.234	-1.038	244.086	-4.536	-0.15	77.516	123.849
4k	-4.501	-1.102	287.043	-4.322	-0.037	81.12	122.501
4l	-5.365	-1.166	249.68	-3.792	0.263	86.072	123.1

Conclusion

New thiadiazoline spiro quinoline derivatives were prepared from quinoline based thiosemicarbazones. The compound structures are characterized by spectroscopic techniques and X-ray crystallographic studies. The cytotoxicity of compounds were examined towards MCF-7 cells and HeLa cells. The synthesized compounds showed good inhibitory activity towards the MCF-7 cells. Amongst, the parent unsbstituted thiadiazoline spiro quinoline compound **4a** exhibited higher activity. The cell death mechanistic studies showeds that the compound **4a** induced apoptosis by inhibition of estrogen receptor alpha (ERα) and G2/M phase cell cycle arrest. The binding affinity and pharmacokinetic properties of the compounds were further evaluated by computational studies. Hence, the potent thiadiazoline spiro quinoline derivative **4a** could serve for breast cancer therapy.

Experimental Section

Chemistry

The analytical grade solvents and chemicals were bought from Loba Chime and Sigma Aldrich. The JASCO FT-IR 4100 spectrometer utilized for record the IR spectrum. The values of IR frequencies were presented in cm^{-1}. The Bruker advance 400 MHz NMR spectrometer employed analyse proton and carbon NMR spectrum. The chemical shift δ values presented in ppm. The Bruker AXS KAPPA APEX-2 diffractometer was used to analyze the single crystal structures. The CHNS elemental analyzer Perkin Elmer 2400 series II was used for elemental analysis.

Synthesis of Thaiadiazoline Spiro Quinolines 4a-b

The 8-nitro quinoline-thiosemicarbazones **3a-l** were synthesized from the reaction of thiosemicarbazides **1a-d** and 8-nitroquinolones **2a-c** in methanol using few drops of acetic acid as catalyst. In the next step, the thiosemicarbazones **3a-l** were refluxed in 20 ml of freshly distilled acetic anhydride at 90 °C for 3 to 5 hours. After completion of the reaction the whole mixture was poured into crushed ice. The obtained products **4a-b** were filtered and recrystaled in methanol.

X-ray crystallographic analysis

All the crystals of the product were acquired by slow evaporation method. The good quality and transparent crystals were analyzed for X-ray crystallographic analysis using 0.71073 Å of X-ray wavelengths. The data of the solved crystals were given in table S1, S2, S3. The crystals ere refined by SHELXL-2014 full-matrix least-squares calculations. Geometrically calculated bond distance of hydrogen atoms are –CH = 0.93 Å (for aromatic), -CH = 0.97 Å (for CH_2) and compelled to ride on the concerned parent atom with $U_{iso}(H)$ = 1.2 or 1.5 U_{eq} (parent atom). The N-H hydrogen was isotropically refined and placed from electro density map. The ORTEP diagram of the compounds was shown in Figure 1.

N-(3'-acetyl-8-nitro-2,3-dihydro-1*H*,3'-spiro [quinoline-4,2'- [1,3,4,] thiadiazol]-5'-yl) acetamide 4a

Yellow solid; yield (96%); mp: 204-212°C; IR (KBr): 3407, 3330, 1704, 1614 cm^{-1}: ^{1}H NMR (400MHz, DMSO-d_6) : δ ppm 11.70 (s, 1H, NH), 8.75 (s, 1H, NH), 7.96 (dd. J = 7.2 Hz, 1H, Ar-H), 7.45 (dd, J = 6.4 Hz, 1H, Ar-H), 6.61 (t, J = 7.2 Hz, 1H, Ar-H). 3.78-3.74 (m, 1H), 3.40-3.29 (m, 1H), 3.13-3.05 (m, 1H), 2.27 (d, J = 7.2Hz, 1H), 2.18 (s, 3H, CH_3), 2.03 (s, 3H, CH_3): ^{13}C NMR (100MHz, DMSO-d_6): δ ppm 22.49, 23.89, 31.29, 38.80, 77.34, 114.49, 125.94, 126.13, 130.93, 132.84, 140.56, 141.25, 167.46, 169.50. Anal. Calcd for: $C_{14}H_{15}N_5O_4S$; C, 48.13, H, 4.33; N, 20.05; O, 18.32; S, 9.18. Found; C, 48.08; H, 4.35; N, 20.01; O, 18.26; S, 9.15.

N-(3'-acetyl-8-nitro-2,3-dihydro-1*H*,3'-spiro [quinoline-4,2'- [1,3,4,] thiadiazol]-5'-yl)-*N*-methylacetamide 4b

Yellow solid; yield (92%); mp: 205-214°C; IR (KBr): 3421, 3328, 1706, 1611 cm^{-1}: ^{1}H NMR (400MHz, DMSO-d_6) : δ ppm 8.49 (d, J = 4.0 Hz, 1H, NH), 7.98(dd, J = 7.6 Hz, 1H, Ar-H), 7.47 (d, J = 7.2 Hz, 1H, Ar-H), 6.63 (t, J = 8.0 Hz, 1H, Ar-H), 3.81-3.75 (m, 1H), 3.46 (s, 3H, CH_3), 3.42-3.35 (m, 1H), 3.12-3.04 (m, 1H), 2.28 (s, 3H, CH_3), 2.26 (s, 1H,), 2.23 (s, 3H, CH_3): ^{13}C NMR (100MHz, DMSO-d_6): δ ppm 22.63, 23.68, 31.12, 38.70, 77.88, 114.46, 125.90, 126.13, 130.91, 132.82, 140.52, 143.25, 167.93, 171.73. Anal. Calcd for: $C_{15}H_{17}N_5O_4S$; C, 49.58, H, 4.72; N, 19.27; O, 17.61; S, 8.82. Found; C, 49.53; H, 4.75; N, 19.18; O, 17.58; S, 8.78.

N-(3'-acetyl-8-nitro-2,3-dihydro-1*H*,3'-spiro [quinoline-4,2'- [1,3,4,] thiadiazol]-5'-yl)-*N*-ethylacetamide 4c

Yellow solid; yield (91%); mp: 206-216°C; IR (KBr): 3411, 3332, 1748, 1613 cm^{-1}: ^{1}H NMR (400MHz, DMSO-d_6) : δ ppm 8.48 (d, J = 2.8 Hz, 1H, NH), 7.98 (dd, J = 7.2 Hz, 1H, Ar-H), 7.47 (d, J = 7.2 Hz, 1H, Ar-

CH), 6.62 (t, *J* = 7.6 Hz, 1H, Ar-H), 3.95-3.93 (m, 2H, CH_2), 3.79-3.75 (m, 1H), 3.40-3.36 (m, 1H), 3.11-3.03 (m, 1H), 3.29 (s, 3H, CH_3), 2.25-2.26 (m, 1H), 2.22 (s, 3H, CH_3), 1.32 (t, *J* = 6.8 Hz, 3H, CH_3): ^{13}C NMR (100MHz, DMSO-d_6): δ ppm 13.39, 22.59, 24.19, 31.57, 39.27, 43.80, 78.19, 114.97, 126.42, 126.56, 131.38, 133.25, 141.01, 142.49, 168.49, 171.66. Anal. Calcd for: $C_{16}H_{19}N_5O_4S$; C, 50.92, H, 5.07; N, 18.56; O, 16.96; S, 8.50. Found; C, 50.89; H, 5.05; N, 18.52; O, 16.91; S, 8.48.

_N_-(3'-acetyl-8-nitro-2,3-dihydro-1_H_,3'-spiro [quinoline-4,2'- [1,3,4,] thiadiazol]-5'-yl)-_N_-phenylacetamide 4d

Yellow solid; yield (92%); mp: 208-218°C; IR (KBr): 3423, 3327, 1708, 1609 cm^{-1}: ^{1}H NMR (400MHz, DMSO-d_6) : δ ppm 8.48 (d, *J* = 4.0 Hz, 1H, NH), 7.97 (dd, *J* = 7.2 Hz, 1H, Ar-H), 7.55-7.43 (m, 6H, Ar-H), 6.65 (t, *J* = 7.6 Hz, 1H, Ar-H), 3.78-3.74 (m, 1H), 3.43-3.36 (m, 1H), 3.05-2.98 (m, 1H), 2.33 (d, *J* = 12.8 Hz, 1H), 1.89 (s, 3H, CH_3), 1.77 (s, 3H, CH_3): ^{13}C NMR (100MHz, DMSO-d_6): δ ppm 23.29, 31.22, 35.93, 38.65, 78.63, 114.50, 125.80, 126.03, 128.67, 129.16, 129.57, 130.95, 132.99, 139.11, 140.60, 144.03, 167.75, 170.54. Anal. Calcd for: $C_{20}H_{19}N_5O_4S$; C, 50.46, H, 4.50; N, 16.46; O, 15.04; S, 8.80. Found; C, 56.41; H, 4.48; N, 16.41; O, 15.01; S, 7.49.

_N_-(3'-acetyl-6-methyl-8-nitro-2,3-dihydro-1_H_,3'-spiro[quinoline-4,2'-[1,3,4,] thiadiazol]-5'-yl) acetamide 4e

Yellow solid; yield (95%); mp: 205-211°C; IR (KBr): 3408, 3324, 1701, 1611 cm^{-1}: ^{1}H NMR (400MHz, DMSO-d_6) : δ ppm 11.71 (s, 1H, NH), 8.36 (d. *J* = 4.0 Hz, 1H, NH), 7.93 (t, *J* = 1.2 Hz, 1H, Ar-H), 7.29 (d, *J* = 1.2 Hz, 1H, Ar-H), 3.76-3.72 (m, 1H), 3.39-3.30 (m, 1H), 3.11-3.04 (m, 1H), 2.26-2.18 (d, *J* = 13.6Hz, 1H), 2.19 (s, 3H, CH_3), 2.09 (s, 3H, CH_3): ^{13}C NMR (100MHz, DMSO-d_6): δ ppm 19.59, 22.40, 23.86, 31.48, 77.30, 123.39, 125.19, 126.11, 130.58, 134.02, 138.96, 141.24, 167.38, 169.47. Anal. Calcd for: $C_{15}H_{17}N_5O_4S$; C, 49.58, H, 4.72; N, 19.27; O, 17.61; S, 8.82. Found; C, 49.54; H, 4.69; N, 19.35; O, 17.62; S, 8.79.

_N_-(3'-acetyl-6-methyl-8-nitro-2,3-dihydro-1_H_,3'-spiro[quinoline-4,2'-[1,3,4,] thiadiazol]-5'-yl)-_N_-methylacetamide 4f

Yellow solid; yield (94%); mp: 206-216°C; IR (KBr): 3402, 3324, 1707, 1611 cm^{-1}: ^{1}H NMR (400MHz, DMSO-d_6) : δ ppm 8.35 (d, *J* = 4.0 Hz, 1H, NH), 7.77(d, *J* = 1.2 Hz, 1H, Ar-H), 7.29 (d, *J* = 4.0 Hz, 1H, Ar-H), 3.74-3.70 (m, 1H), 3.44 (s, 3H), 3.38-3.30 (m, 1H), 3.07-2.99 (m, 1H), 2.26 (s, 3H, CH_3), 2.21 (s, 3H, CH_3), 2.17 (s, 3H, CH_3): ^{13}C NMR (100 MHz, DMSO-d_6): δ ppm 19.64, 22.63, 23.67, 31.36, 35.10, 38.52, 77.87, 123.40, 125.17, 126.04, 130.61, 134.12, 138.98, 143.28, 167.84, 171.13. Anal. Calcd for: $C_{16}H_{19}N_5O_4S$; C, 50.92, H, 5.07; N, 18.56; O, 16.96; S, 8.50. Found; C, 50.90; H, 5.09; N, 18.53; O, 16.91; S, 8.49.

_N_-(3'-acetyl-6-methyl-8-nitro-2,3-dihydro-1_H_,3'-spiro[quinoline-4,2'-[1,3,4,] thiadiazol]-5'-yl)-_N_-ethylacetamide 4g

Yellow solid; yield (93%); mp: 207-215°C; IR (KBr): 3398, 3332, 1701, 1613 cm^{-1}: ^{1}H NMR (400MHz, DMSO-d_6) : δ ppm 8.38 (d, *J* = 4.0 Hz, 1H, NH), 7.80(s, 1H, Ar-H), 7.31 (s, 1H Ar-H), 4.01-3.90 (m, 2H), 3.76-

3.72 (m, 1H), 3.40-3.32 (m, 1H), 3.09-3.01 (m, 1H), 2.30 (s, 3H, CH_3), 2.27-2.26 (m, 1H), 2.24 (s, 3H, CH_3), 2.20 (s, 3H, CH_3), 1.34 (t, *J* = 8.0 Hz, 3H, CH_3): ^{13}C NMR (100MHz, DMSO-d_6): δ ppm 12.90, 19.65, 22.10, 23.68, 31.27, 38.62, 43.30, 78.05, 123.38, 125.21, 125.78, 130.60, 133.98, 138.98, 142.07, 167.95, 171.15. Anal. Calcd for: $C_{17}H_{21}N_5O_4S$; C, 52.16, H, 5.41; N, 17.89; O, 16.35; S, 8.19. Found; C, 52.15; H, 5.39; N, 17.84; O, 16.33; S, 8.17.

N-(3'-acetyl-6-methyl-8-nitro-2,3-dihydro-1*H*,3'-spiro[quinoline-4,2'-[1,3,4,] thiadiazol]-5'-yl)-*N*-phenylacetamide 4h

Yellow solid; yield (92%); mp: 204-212°C; IR (KBr): 3403, 3326, 1698, 1606 cm^{-1}: ^{1}H NMR (400MHz, DMSO-d_6) : δ ppm 8.37 (d, *J* = 4.0 Hz, 1H), 8.08(d, *J* = 1.2 Hz, 1H), 7.56-7.49 (m, 5H Ar-H), 7.30 (d, *J* = 2.0 Hz, 1H, Ar-H), 3.76-3.70 (m, 1H), 3.45-3.35 (m, 1H), 3.03-2.95 (d, J = 4.0 Hz, 1H), 2.32 (d, *J* = 12.8 Hz, 1H), 2.19 (s, 3H, CH_3), 1.90 (s, 3H, CH_3), 1.78 (s, 3H, CH_3): ^{13}C NMR (100MHz, DMSO-d_6): δ ppm 19.61, 23.25, 31.33, 38.46, 78.03, 123.37, 125.29, 125.60, 128.64, 129.13, 129.54, 130.60, 134.20, 139.02, 139.10, 144.03, 167.68, 170.51. Anal. Calcd for: $C_{21}H_{21}N_5O_4S$; C, 57.39, H, 4.82; N, 15.94; O, 14.56; S, 7.30. Found; C, 57.36; H, 4.81; N, 15.92; O, 14.51; S, 7.25.

N-(3'-acetyl-6-chloro-8-nitro-2,3-dihydro-1*H*,3'-spiro [quinoline-4,2'-[1,3,4,] thiadiazol]-5'-yl) acetamide 4i

Yellow solid; yield (96%); mp: 207-218°C; IR (KBr): 3411, 3328, 1707, 1618 cm^{-1}: ^{1}H NMR (400MHz, DMSO-d_6) : δ ppm 11.78 (s, 1H, NH), 8.59 (d, *J* = 4.0Hz, 1H, NH), 7.99 (d. J = 4.0 Hz, 1H, Ar-H), 7.43 (d, *J* = 2.4 Hz, 1H, Ar-H), 3.81-3.74 (m, 1H), 3.41-3.34 (m, 1H), 3.07-2.99 (m, 1H), 2.30 (d, *J* = 16.0Hz, 1H), 2.22 (s, 3H, CH_3), 2.06 (s, 3H, CH_3): ^{13}C NMR (100MHz, DMSO-d_6): δ ppm 22.41, 23.84, 30.94, 38.62, 76.78, 117.55, 124.80, 128.28, 131.01, 132.14, 139.62, 141.36, 167.59, 169.62. Anal. Calcd for: $C_{14}H_{24}N_5O_4S$; C, 43.81, H, 3.68; Cl, 9.24; N, 18.25; O, 16.67; S, 8.35. Found; C, 43.79; H, 3.65; Cl, 9.23; N, 18.22; O, 16.69; S, 8.31.

N-(3'-acetyl-6-chloro-8-nitro-2,3-dihydro-1*H*,3'-spiro [quinoline-4,2'-[1,3,4,] thiadiazol]-5'-yl)-*N*-methylacetamide 4j

Yellow solid; yield (94%); mp: 206-218°C; IR (KBr): 3421, 3327, 1706, 1611 cm^{-1}: ^{1}H NMR (400MHz, DMSO-d_6) : δ ppm 8.57 (d, *J* = 4.0 Hz, 1H, NH), 7.97(d, *J* = 2.4 Hz, 1H, Ar-H), 7.40 (d, *J* = 2.4 Hz, 1H, Ar-H), 3.77-3.75 (m, 1H, CH_3), 3.45 (s, 3H, CH_3), 3.39-3.32 (m, 1H), 3.30-2.95 (m, 1H), 2.28 (s, 3H, CH_3), 2.23 (s, 3H, CH_3): ^{13}C NMR (100MHz, DMSO-d_6): δ ppm 22.55, 23.57, 30.79, 35.10, 38.49, 77.28, 117.51, 124.72, 128.26, 130.98, 132.13, 139.56, 143.31, 167.98, 171.84. Anal. Calcd for: $C_{15}H_{16}ClN_5O_4S$; C, 45.29, H, 4.05; Cl, 8.91; N, 17.60; O, 16.09; S, 8.06. Found; C,45.27; H, 4.01; Cl, 8.87; N, 17.59; O, 16.11; S, 8.05.

N-(3'-acetyl-6-chloro-8-nitro-2,3-dihydro-1*H*,3'-spiro [quinoline-4,2'-[1,3,4,] thiadiazol]-5'-yl)-*N*-ethylacetamide 4k

Yellow solid; yield (93%); mp: 208-218°C; IR (KBr): 3414, 3332, 1708, 1613 cm^{-1}: ^{1}H NMR (400MHz, DMSO-d_6) : δ ppm 8.57 (d, J = 4.0 Hz, 1H, NH), 7.97(d, J = 2.4 Hz, 1H, Ar-H), 7.42 (d, J = 2.4 Hz, 1H, Ar-H), 3.98-3.91 (m, 2H), 3.77-3.73 (m, 1H), 3.39-3.36 (m, 1H), 3.02-2.94 (m, 1H), 2.30 (s, 3H, CH_3), 2.23 (s, 3H, CH_3), 1.33 (t, J = 8.0 Hz, 3H, CH_3): ^{13}C NMR (100MHz, DMSO-d_6): δ ppm 12.83, 22.01, 23.57, 30.70, 38.54, 43.33, 77.36, 117.50, 124.75, 128.11, 132.06, 142.37, 166.56, 172.11. Anal. Calcd for: $C_{16}H_{18}ClN_5O_4S$; C, 46.66, H, 4.41; Cl, 8.61; N, 17.00; O, 15.54; S, 7.79. Found; C, 46.68; H, 4.40; Cl, 8.57; N, 17.01; O, 15.51; S, 7.76.

N-(3'-acetyl-6-chloro-8-nitro-2,3-dihydro-1*H*,3'-spiro[quinoline-4,2'- [1,3,4,] thiadiazol]-5'-yl)-*N*-phenylacetamide 4i

Yellow solid; yield (92%); mp: 205-213°C; IR (KBr): 3412, 3325, 1707, 1611 cm^{-1}: ^{1}H NMR (400MHz, DMSO-d_6) : δ ppm 8.58 (d, J = 4.0 Hz, 1H, NH), 7.99(d, J = 4.0 Hz, 1H, Ar-H), 7.57-7.43 (m, 5H Ar-H), 3.78-3.76 (m, 1H), 3.42-3.37 (m, 1H), 3.17 (d, J = 4.0 Hz, 1H), 2.97-2.90 (m, 1H), 2.34 (d, J = 12.0 Hz, 1H), 1.90 (s, 3H, CH_3), 1.79 (s, 3H, CH_3): ^{13}C NMR (100MHz, DMSO-d_6): δ ppm 22.94, 23.22, 30.87, 38.39, 77.93, 117.52, 124.84, 127.83, 128.67, 129.18, 129.54, 131.00, 132.37, 139.02, 139.68 144.16, 167.78, 170.65. Anal. Calcd for: $C_{20}H_{18}ClN_5O_4S$; C, 46.66, H, 4.41; Cl, 8.61; N, 17.00; O, 15.54; S, 7.79. Found; C, 46.68; H, 4.40; Cl, 8.57; N, 17.01; O, 15.51; S, 7.76.

Biology

MTT Cytotoxicity Study

The MTT (3-4,5-dimethylthiazol-2-yl)-2,5-diphenyltetrazoliumbromide) was utilized to examine the cytotoxicity of synthesized compounds. The MCF-7 and HeLa cells were purchased from National Centre for Cell Science (NCCS) Pune. The HeLa and MCF-7 cells were placed in growth medium containing 96 well plates. The compounds were serially diluted and seeded to cells containing wells for 24 hours at 37°C and moisten with 5% CO_2. Then the growth medium was suctioned and altered with MTT. After 4 hours incubation the MTT also removed and the acidified ethanol was added for the lysis step. The spectrometer was used to analyze the cell viability. The experiment was repeated three times as triplicate and then the IC_{50} was determined from absorbance values.

AO/EB Dual staining assay

The apoptosis induced by the compounds was found by AO/EB dual staining process. The MCF-7 cancer cells were placed and developed in 24-well plate. Then 25μM and 50μM of the compound 4a was added to the cells and keep alive for one day. After that the treated cells were washed with PBS and stained with 5μg/mL of AO/EB for 1 hour. The stained cells were again washed with PBS and examined by Nikon ECLIPSE, TS 100 fluorescence microscopy (excitation at 480/30 nm) to distinguish the apoptotic cells.

DAPI Staining Method

The compound induced nuclear damage in the treated cells was found by DAPI staining method. The MCF-7 cancer cells were placed and developed in 24-well plate. Then 25μM and 50μM of the compound 4a was added to the cells and keep alive for one day. After that the treated cells were washed with PBS and stained with 5μg/mL of DAPI for 1 hour. The stained cells were again washed with PBS and examined by Nikon ECLIPSE, TS 100 fluorescence microscopy (excitation at 510 nm) to distinguish the apoptotic nuclear damage.

Cell Cycle Analysis

The flow cytometry method is used to examine the cell cycle. The MCF-7 cancer cells were placed and developed in 24-well plate. Then IC_{50} concentration of the compound 4a was added to the cells and keeps alive for one day. After that the treated cells were washed with PBS and stained with 50 mg/mL of propidium iodide for 30 minutes. After staining the cells were examined by flow cytometry (BD bioscience, San Jose, CA, USA) for cell cycle distribution and DNA content.

Annexin V- FITC and PI Staining Assay

The apoptotic cells were quantitatively analyzed by flow cytometry annexin V-FITC and PI staining method. The MCF-7 cancer cells were placed and developed in 24-well plate. Then IC_{50} concentration of the compound 4a was added to the cells and keeps alive for one day. After that the treated cells were suspended with binding buffer (200μL). Then the cells were stained with 5μL of propidium iodide and 10μL of annexin V-FITC for 30 minutes. After staining the cells were examined by flow cytometry (BD FACS caliber, USA) to quantify the apoptotic cells.

Gene expression analysis by RT-PCR

The reverse transcriptase- poly chain reaction RT-PCR method was used to examine the ERα levels. The MCF-7 cancer cells were placed and developed in 24-well plate. Then IC_{50} concentration of the compound 4a was added to the cells and incubated for 24 hours. After that the levels of ERα in the treated cell was analysed by RT-PCR method and the β-actin was used as internal control. The conventional thiazole method was used to isolate the total RNA from the treated cancer cells. The cDNA conversion of separated RNA was performed by reverse transcription of M-MLV reverse transcriptase. From the RT product the level of β-actin and ERα was quantified using semi-quantitative PCR ananlysis. The agarose gel was used to resolve the PCR product then then ethidium bromide was used to stain the resolved products to visualized in UV light. The experiment was repeated thrice as triplicate and the primers used were

Estrogen Receptor alpha ERα

Forward primer: 50 GTGCCTGGCTAGAGATCCTC 30

Reverse primer: 30 GATGTGGGAGAGGATGAGGA 50.

β-actin

Forward primer: 5´- CTGTCTGGCGGCACCACCAT-3´

Reverse primer: 5´- GCAACTAAGTCATAGTCCG-3´.

Western blot analysis

The western blot method is used to analyze the level of ERα protein. The MCF-7 cancer cells were placed and developed in 24-well plate. Then IC_{50} concentration of the compound 4a was added to the cells and incubated for 24 hours. The treated cells were washed with PBS and lysed with SDS (sodium dodecyl sulfate). The 10% SDS-PAGE gels was used to resolve the proteins from the lysates. The Gels were moved on nitrocellulose membranes and blocked with 5% of non-fat dry milk, incubated with primary antibodies of rabbit anti-ERα (1: 1000, CST) and, mouse antibody anti-β-actin. Then the membrane was washed with PBS. Then the goat anti-rabbit secondary antibody was added to the washed membrane and incubated for 1 hour. After incubation, the membranes were washed and examined by enhanced chemiluminescence ECL.

References

1 Bray, F. *et al.* Global cancer statistics 2018: GLOBOCAN estimates of incidence and mortality worldwide for 36 cancers in 185 countries. *Ca-a Cancer Journal for Clinicians* **68**, 394-424, doi:10.3322/caac.21492 (2018).

2 Chantalat, E. *et al.* The AF-1-deficient estrogen receptor ER alpha 46 isoform is frequently expressed in human breast tumors. *Breast Cancer Research* **18**, doi:10.1186/s13058-016-0780-7 (2016).

3 Li, Y. J., Geng, J. K., Liu, Y., Yu, S. H. & Zhao, G. S. Thiadiazole-a Promising Structure in Medicinal Chemistry. *Chemmedchem* **8**, 27-41, doi:10.1002/cmdc.201200355 (2013).

4 Jain, A. K., Sharma, S., Vaidya, A., Ravichandran, V. & Agrawal, R. K. 1,3,4-Thiadiazole and its Derivatives: A Review on Recent Progress in Biological Activities. *Chemical Biology & Drug Design* **81**, 557-576, doi:10.1111/cbdd.12125 (2013).

5 Busch, B. B. *et al.* Identification of a selective inverse agonist for the orphan nuclear receptor estrogen-related receptor alpha. *Journal of Medicinal Chemistry* **47**, 5593-5596, doi:10.1021/jm049334f (2004).

6 Willy, P. J. *et al.* Regulation of PPAR gamma coactivator 1 alpha (PGC-1 alpha) signaling by an estrogen-related receptor alpha (ERR alpha) ligand. *Proceedings of the National Academy of Sciences of the United States of America* **101**, 8912-8917, doi:10.1073/pnas.0401420101 (2004).

7 Finlay, M. R. V. *et al.* Discovery of a Thiadiazole-Pyridazine-Based Allosteric Glutaminase 1 Inhibitor Series That Demonstrates Oral Bioavailability and Activity in Tumor Xenograft Models. *Journal of Medicinal Chemistry* **62**, 6540-6560, doi:10.1021/acs.jmedchem.9b00260 (2019).

8 Aurelio, L. *et al.* From Sphingosine Kinase to Dihydroceramide Desaturase: A Structure-Activity Relationship (SAR) Study of the Enzyme Inhibitory and Anticancer Activity of 4-((4-(4-Chlorophenyl)thiazol-2-yl)amino)phenol (SKI-II). *Journal of Medicinal Chemistry* **59**, 965-984, doi:10.1021/acs.jmedchem.5b01439 (2016).

9 Zhang, L., Zhao, J. Y., Zhang, B. C., Lu, T. & Chen, Y. D. Discovery of 1,2,4 triazolo 3,4-b 1,3,4 thiadiazole derivatives as novel, potent and selective c-Met kinase inhibitors: Synthesis, SAR study, and biological activity. *European Journal of Medicinal Chemistry* **150**, 809-816, doi:10.1016/j.ejmech.2018.03.049 (2018).

10 Talapatra, S. K. *et al.* Crystal structure of the Eg5-K858 complex and implications for structure-based design of thiadiazole-containing inhibitors. *European Journal of Medicinal Chemistry* **156**, 641-651, doi:10.1016/j.ejmech.2018.07.006 (2018).

11 Wang, W. L. *et al.* Benzo c 1,2,5 thiadiazole derivatives: A new class of potent Src homology-2 domain containing protein tyrosine phosphatase-2 (SHP2) inhibitors. *Bioorganic & Medicinal Chemistry Letters* **27**, 5154-5157, doi:10.1016/j.bmcl.2017.10.059 (2017).

12 Raj, V. *et al.* Novel 1,3,4-thiadiazoles inhibit colorectal cancer via blockade of IL-6/COX-2 mediated JAK2/STAT3 signals as evidenced through data-based mathematical modeling. *Cytokine* **118**, 144-159, doi:10.1016/j.cyto.2018.03.026 (2019).

13 Parveen, I., Ahmed, N., Idrees, D., Khan, P. & Hassan, M. I. Synthesis, estrogen receptor binding affinity and molecular docking of pyrimidine-piperazine-chromene and - quinoline conjugates. *Bioorganic & Medicinal Chemistry Letters* **27**, 4493-4499, doi:10.1016/j.bmcl.2017.07.077 (2017).

14 Burks, H. E. *et al.* Discovery of an Acrylic Acid Based Tetrahydroisoquinoline as an Orally Bioavailable Selective Estrogen Receptor Degrader for ER alpha plus Breast Cancer. *Journal of Medicinal Chemistry* **60**, 2790-2818, doi:10.1021/acs.jmedchem.6b01468 (2017).

15 Kundu, B. *et al.* Discovery and Mechanistic Study of Tailor-Made Quinoline Derivatives as Topoisomerase 1 Poison with Potent Anticancer Activity. *Journal of Medicinal Chemistry* **62**, 3428-3446, doi:10.1021/acs.jmedchem.8b01938 (2019).

16 Lee, H. Y. *et al.* (N-Hydroxycarbonylbenylamino)quinolines as Selective Histone Deacetylase 6 Inhibitors Suppress Growth of Multiple Myeloma in Vitro and in Vivo. *Journal of Medicinal Chemistry* **61**, 905-917, doi:10.1021/acs.jmedchem.7b01404 (2018).

17 Wu, Y. *et al.* Discovery of 2-(4-chloro-3-(trifluoromethyl)phenyl)-N-(4-((6,7-dimethoxyquinolin-4-yl)oxy)phenyl)acetamide (CHMFL-KIT-64) as a Novel Orally Available Potent Inhibitor against Broad Spectrum Mutants of c-KIT Kinase for Gastrointestinal Stromal Tumors. *Journal of Medicinal Chemistry* **62**, 6083-6101, doi:10.1021/acs.jmedchem.9b00280 (2019).

18 Degorce, S. L. *et al.* Discovery of Novel 3-Quinoline Carboxamides as Potent, Selective, and Orally Bioavailable Inhibitors of Ataxia Telangiectasia Mutated (ATM) Kinase. *Journal of Medicinal Chemistry* **59**, 6281-6292, doi:10.1021/acs.jmedchem.6b00519 (2016).

19 Pike, K. G. *et al.* The Identification of Potent, Selective, and Orally Available Inhibitors of Ataxia Telangiectasia Mutated (ATM) Kinase: The Discovery of AZD0156 (8-{6- 3-(Dimethylamino)propoxy pyridin-3-yl}-3-methyl-1-(tetrahydro-2H- pyran-4-yl)-1,3-dihydro-2H-imidazo 4,5-c quinolin-2-one). *Journal of Medicinal Chemistry* **61**, 3823-3841, doi:10.1021/acs.jmedchem.7b01896 (2018).

20 Nepali, K. *et al.* Amide-tethered quinoline-resorcinol conjugates as a new class of HSP90 inhibitors suppressing the growth of prostate cancer cells. *Bioorganic Chemistry* **91**, doi:10.1016/j.bioorg.2019.103119 (2019).

21 Vyas, V. K. *et al.* Synthesis of 2-,4,-6-, and/or 7-substituted quinoline derivatives as human dihydroorotate dehydrogenase (hDHODH) inhibitors and anticancer agents: 3D QSAR-assisted design. *Bioorganic & Medicinal Chemistry Letters* **29**, 917-922, doi:10.1016/j.bmcl.2019.01.038 (2019).

22 Szabadkai, I. *et al.* Discovery of N- 4-(Quinolin-4-yloxy)phenyl benzenesulfonamides as Novel AXL Kinase Inhibitors. *Journal of Medicinal Chemistry* **61**, 6277-6292, doi:10.1021/acs.jmedchem.8b00672 (2018).

23 Lin, J. *et al.* Discovery and Optimization of Quinolinone Derivatives as Potent, Selective, and Orally Bioavailable Mutant Isocitrate Dehydrogenase 1 (mIDH1) Inhibitors. *Journal of Medicinal Chemistry* **62**, 6575-6596, doi:10.1021/acs.jmedchem.9b00362 (2019).

24 Dayal, N. *et al.* Potently inhibiting cancer cell migration with novel 3H-pyrazolo 4,3-f quinoline boronic acid ROCK inhibitors. *European Journal of Medicinal Chemistry* **180**, 449-456, doi:10.1016/j.ejmech.2019.06.089 (2019).

25 Yang, S. M. *et al.* Discovery of Orally Bioavailable, Quinoline-Based Aldehyde Dehydrogenase 1A1 (ALDH1A1) Inhibitors with Potent Cellular Activity. *Journal of Medicinal Chemistry* **61**, 4883-4903, doi:10.1021/acs.jmedchem.8b00270 (2018).

26 Shyamsivappan, S. *et al.* Synthesis and X-ray study of dispiro 8-nitroquinolone analogues and their cytotoxic properties against human cervical cancer HeLa cells. *Medchemcomm* **10**, 439-449, doi:10.1039/c8md00482j (2019).

27 Arasakumar, T. *et al.* Biologically active perspective synthesis of heteroannulated 8-nitroquinolines with green chemistry approach. *Bioorganic & Medicinal Chemistry Letters* **27**, 1538-1546, doi:10.1016/j.bmcl.2017.02.042 (2017).

28 Shyamsivappan, S. *et al.* A novel 8-nitro quinoline-thiosemicarbazone analogues induces G1/S & G2/M phase cell cycle arrest and apoptosis through ROS mediated mitochondrial pathway. *Bioorganic Chemistry* **97**, doi:10.1016/j.bioorg.2020.103709 (2020).

29 Shyamsivappan, S. *et al.* Novel phenyl and thiophene dispiro indenoquinoxaline pyrrolidine quinolones induced apoptosisviaG1/S and G2/M phase cell cycle arrest in MCF-7 cells. *New Journal of Chemistry* **44**, 15031-15045, doi:10.1039/d0nj02588g (2020).

30 Bernstein, J., Davis, R. E., Shimoni, L. & Chang, N. L. PATTERNS IN HYDROGEN BONDING - FUNCTIONALITY AND GRAPH SET ANALYSIS IN CRYSTALS. *Angewandte Chemie-International Edition* **34**, 1555-1573, doi:10.1002/anie.199515551 (1995).

31 Atale, N., Gupta, S., Yadav, U. C. S. & Rani, V. Cell-death assessment by fluorescent and nonfluorescent cytosolic and nuclear staining techniques. *Journal of Microscopy* **255**, 7-19, doi:10.1111/jmi.12133 (2014).

32 Liao, X. H. *et al.* Estrogen receptor alpha mediates proliferation of breast cancer MCF-7 cells via a p21/PCNA/E2F1-dependent pathway. *Febs Journal* **281**, 927-942, doi:10.1111/febs.12658 (2014).

33. Maestro, version 9.3, Schrodinger, LLC, New York, (2012).

34. LigPrep, version 2.5, Schrodinger, LLC, New York, (2012).

35. Glide, version 5.8, Schrodinger, LLC, New York, (2012).

36. QikProp, version 3.5, Schrodinger, LLC, New York, NY, (2014).

Figures

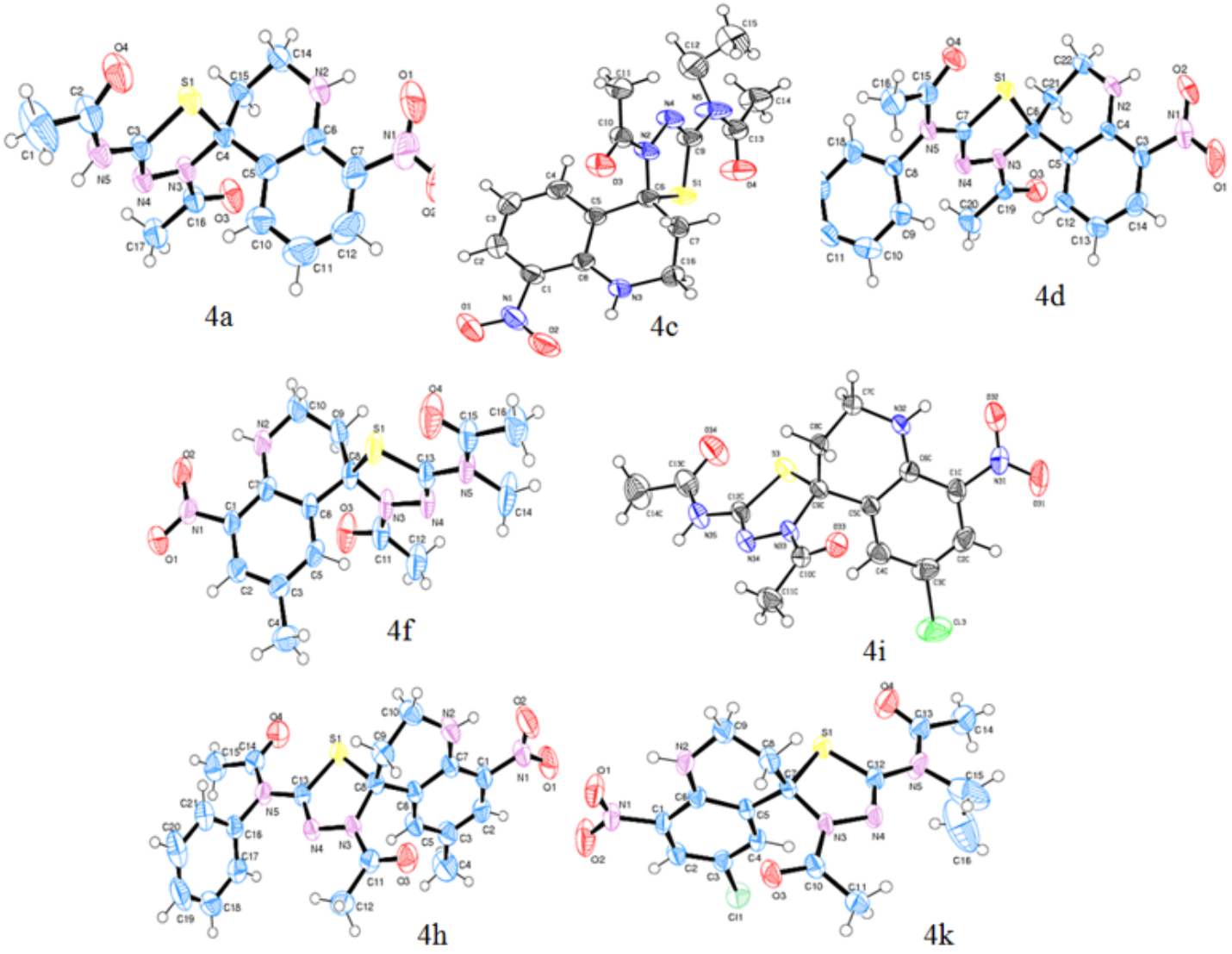

Figure 1

The ORTEP diagram of the compounds 4a, 4c, 4d, 4f, 4h, 4i and 4k

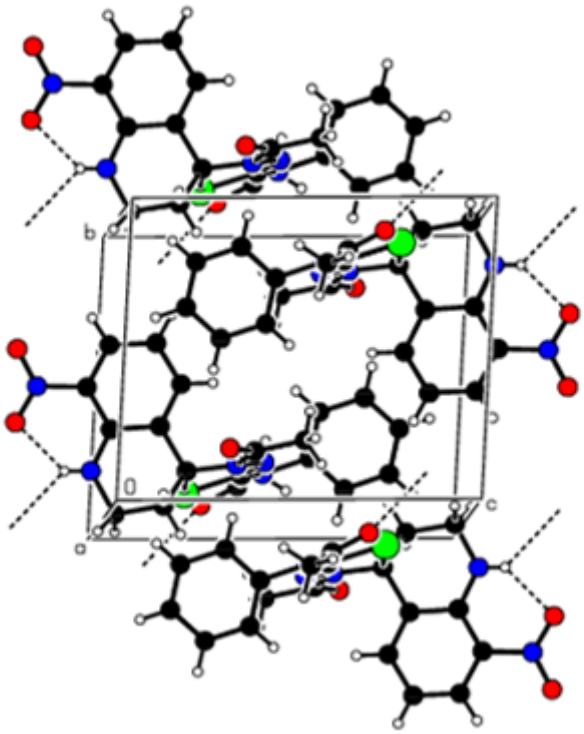

Figure 2

Packing of the molecules showed flat aggregation along ab-plane in the monoclinic unit cell is seen down along a-axis. The dashed lines are indicating the hydrogen bonds.

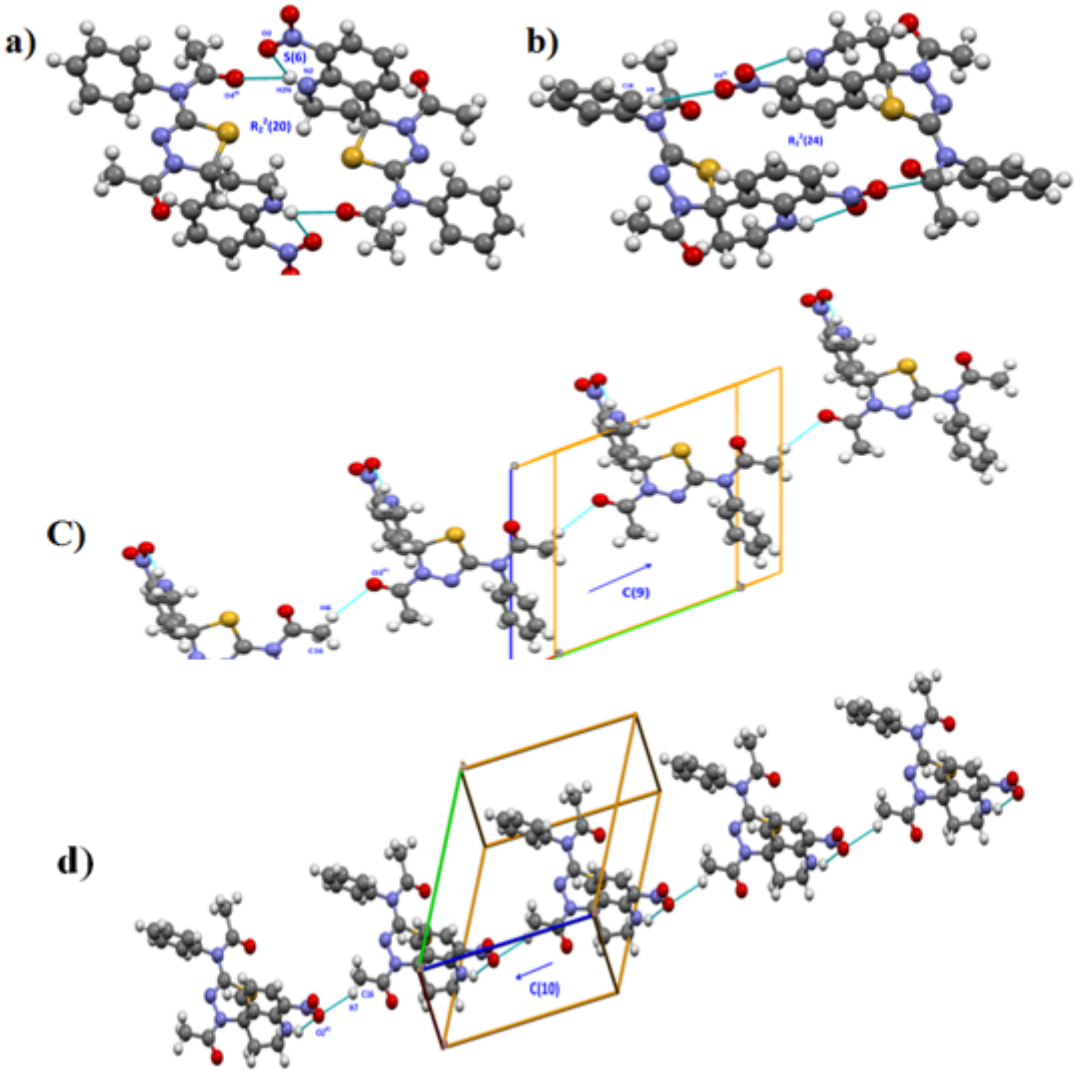

Figure 3

a & b shows the ring motifs; c & d shows the chain motifs. The dashed lines are indicating the hydrogen bonds.

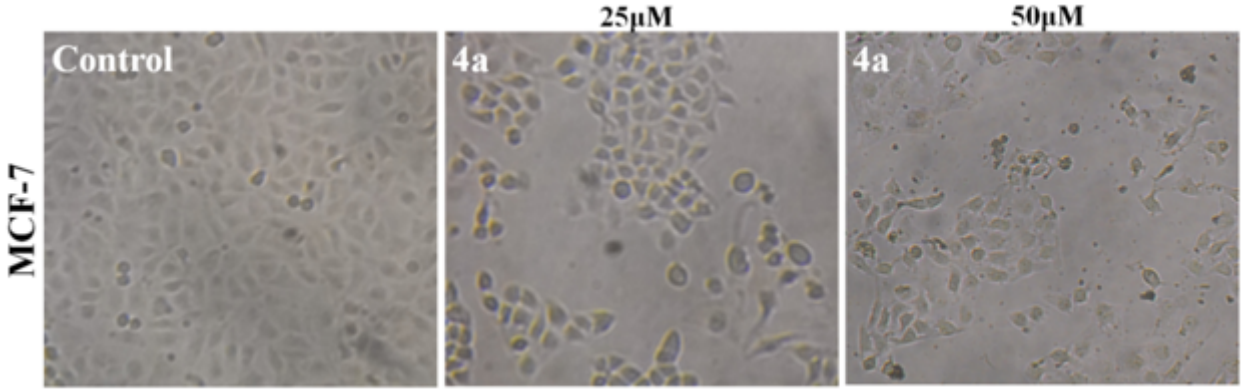

Figure 4

Cell morphology analysis by using phase contrast microscopy. Cell morphology analysis by using phase contrast microscopy

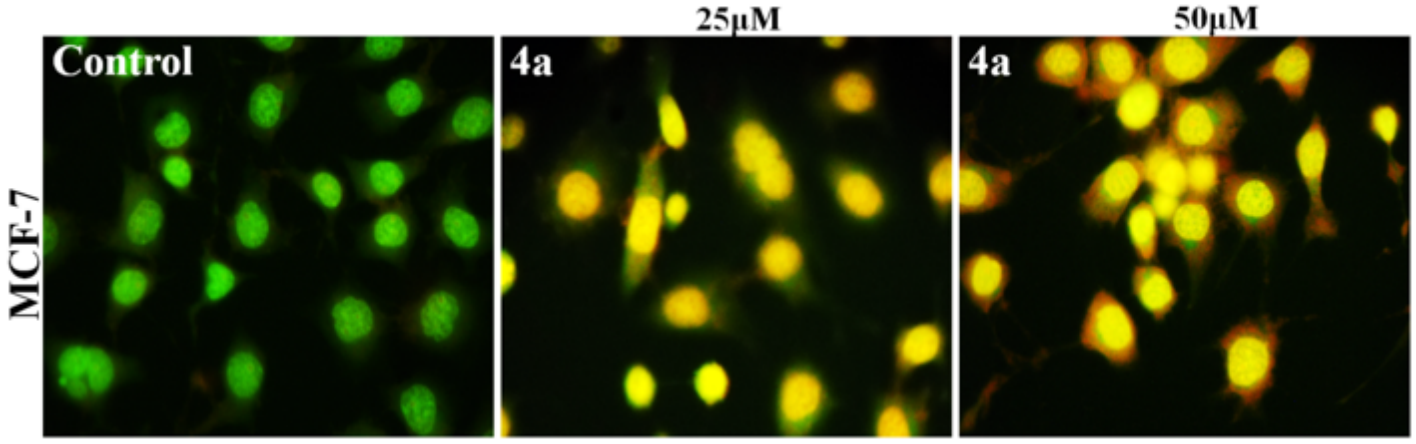

Figure 5

AO/EB analysis for detection of apoptotic cells using fluorescence microscopy.

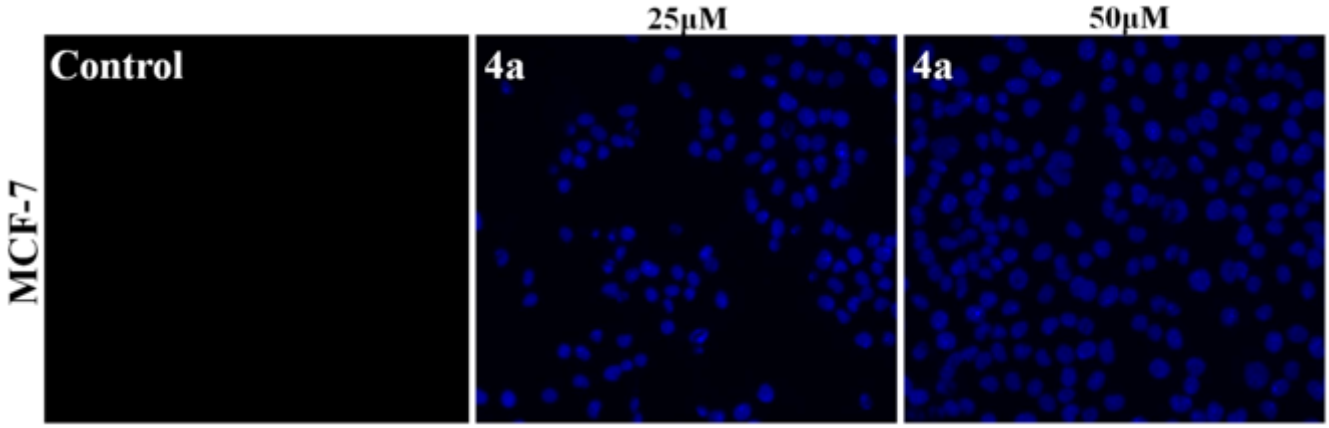

Figure 6

DAPI staining analysis detection apoptotic nuclear damaged cells in the compound 4a treated MCF-7 cells.

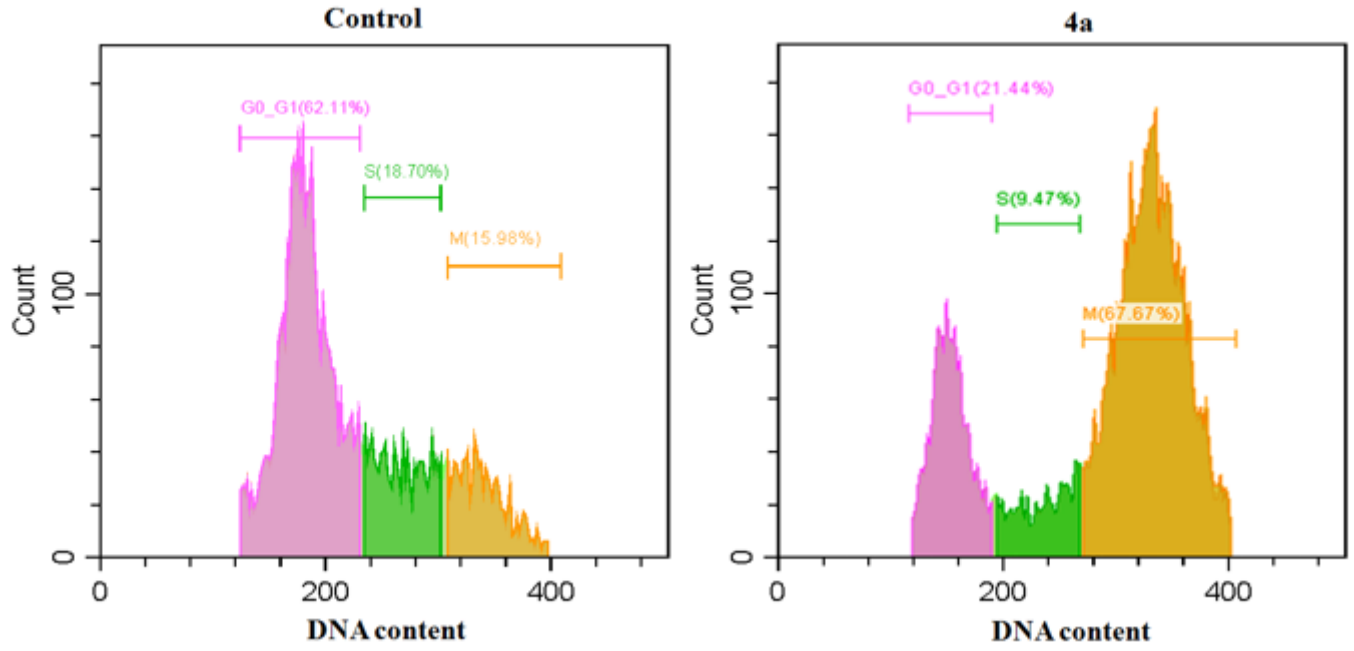

Figure 7

Flow cytometry analysis for detection of cell cycle tested ERα positive MCF-7 cells.

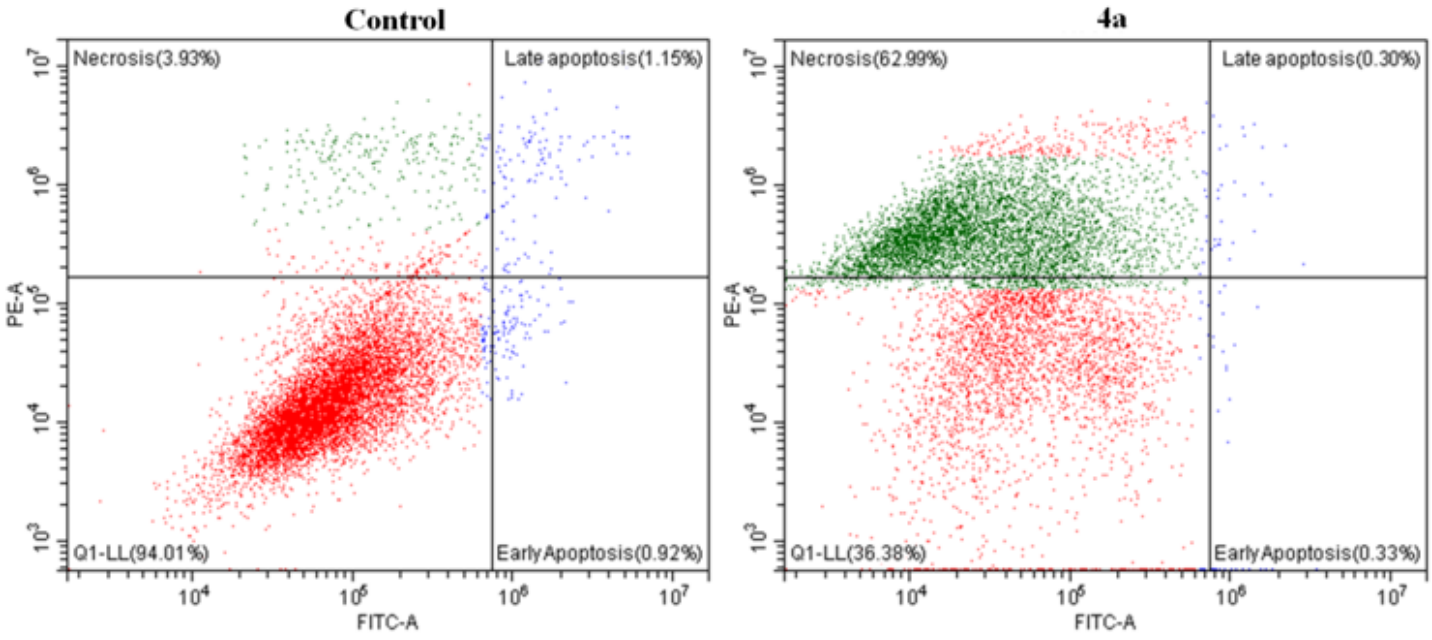

Figure 8

Quantification of apoptotic cells in the compound 4a treated MCF-7 cells by annexin V-FITC and PI staining method

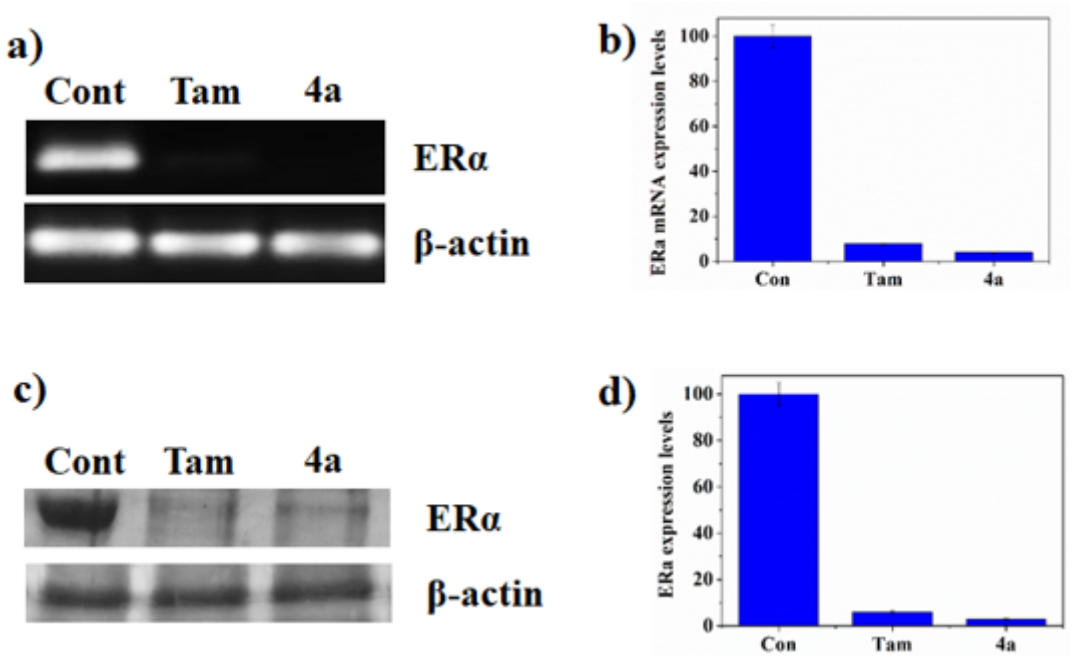

Figure 9

Determination of the level of endogenous ERα in the compound 4a treated MCF-7 cells. a) ERα gene expression analysis by RT-PCR b) Densitometric analysis for ERα gene expressions c) ERα expression analysis by western blot method d) Densitometric analysis for ERα protein expressions

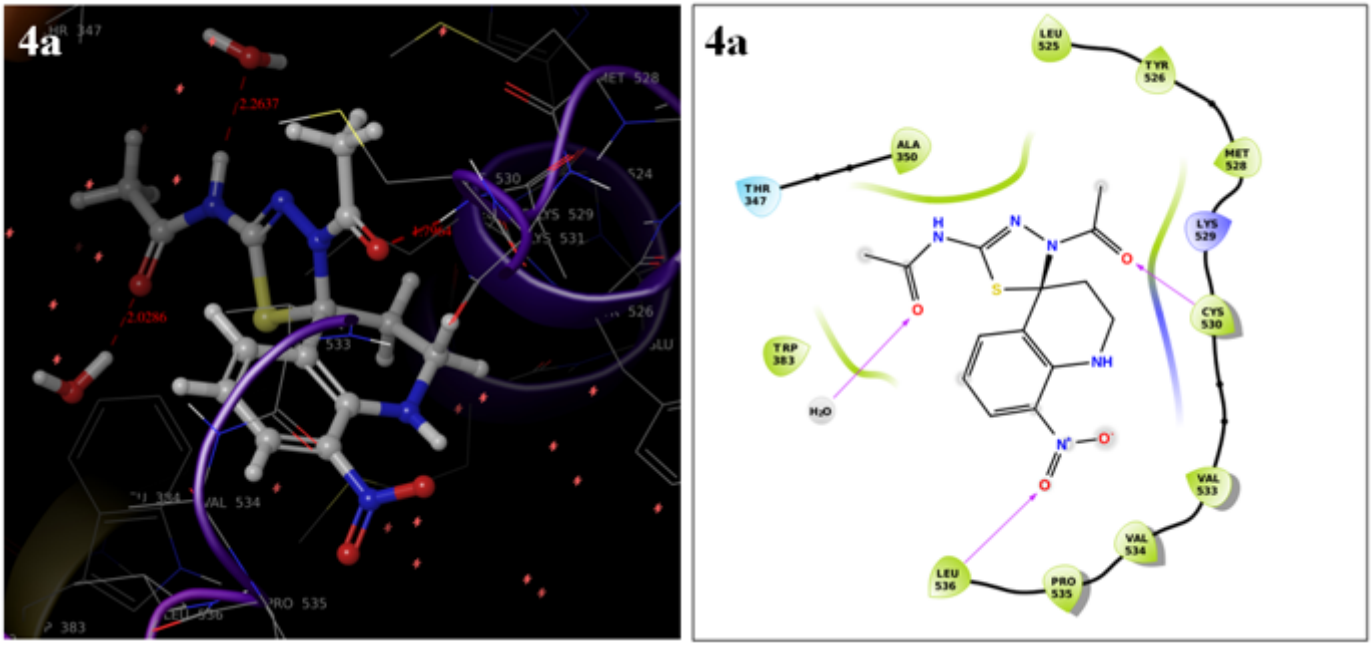

Figure 10

3-dimensional 3D and 2-dimensional 2D molecular interaction pictures of the compound 4a with ERα. The hydrogen bond interactions were mentioned by red arrows.

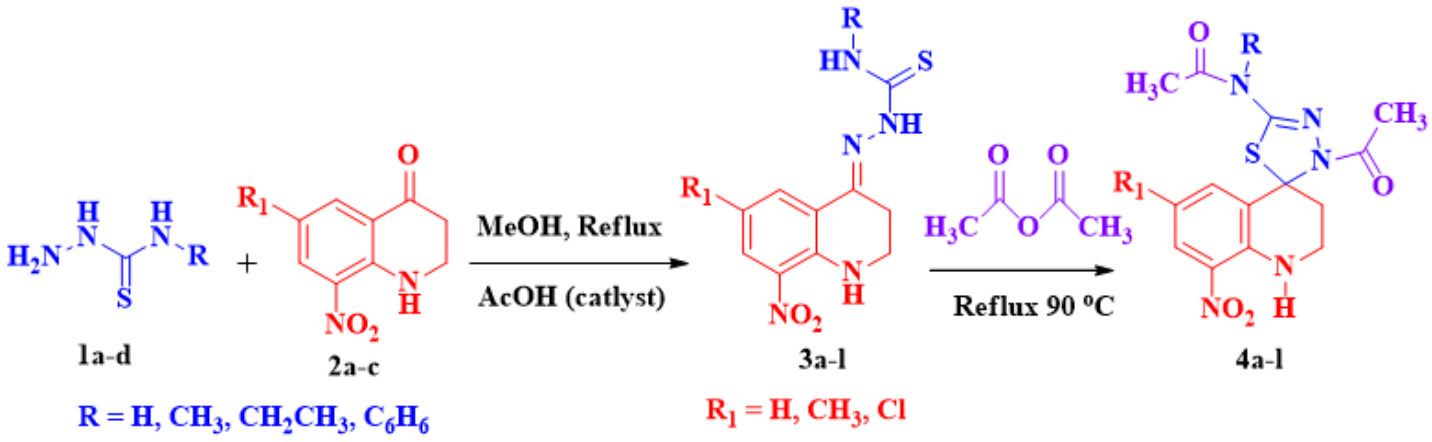

Figure 11

Scheme 1. Synthesis of thiadiazoline spiro quinoline analogues 4a-l

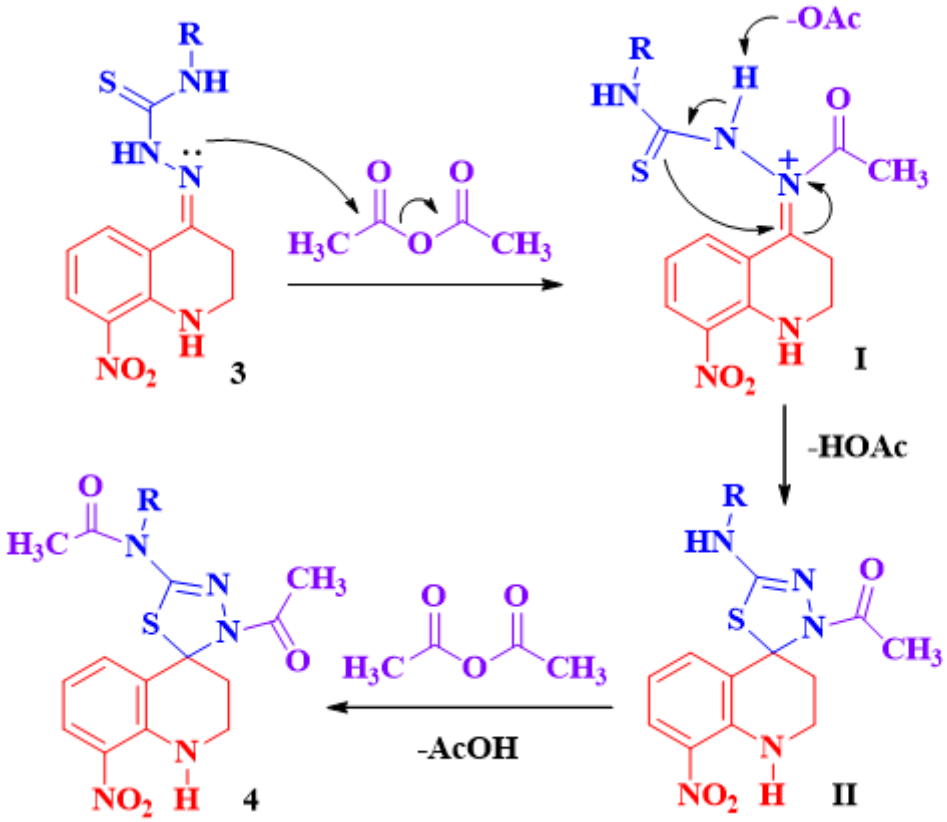

Figure 12

Scheme 2. A convincible mechanism for the development of thiasiazoline spiro quinolines 4a-l

Supplementary Files

This is a list of supplementary files associated with this preprint. Click to download.

- SupportingInformation.docx
- GraphicalAbstract.png